IEEE Photonics Journal
An IEEE Photonics Society Publication

Open Access

Angle-of-Arrival (AOA) Visible Light Positioning (VLP) System Using Solar Cells With Third-Order Regression and Ridge Regression Algorithms

Volume 12, Number 3, June 2020

Chong-You Hong
Yu-Chun Wu
Yang Liu
Chi-Wai Chow
Chien-Hung Yeh
Ke-Ling Hsu
Dong-Chang Lin
Xin-Lan Liao
Kun-Hsien Lin
Yi-Yuan Chen

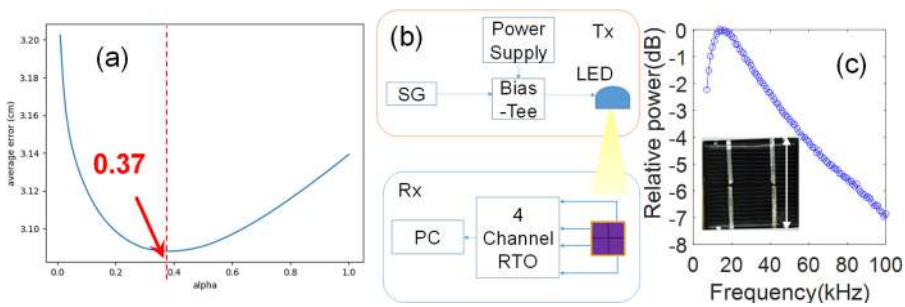

DOI: 10.1109/JPHOT.2020.2993031

Angle-of-Arrival (AOA) Visible Light Positioning (VLP) System Using Solar Cells With Third-Order Regression and Ridge Regression Algorithms

Chong-You Hong,[1] Yu-Chun Wu,[1] Yang Liu,[2] Chi-Wai Chow,[1] Chien-Hung Yeh,[3] Ke-Ling Hsu,[1] Dong-Chang Lin,[1] Xin-Lan Liao,[4] Kun-Hsien Lin,[4] and Yi-Yuan Chen[4]

[1]Department of Photonics, College of Electrical and Computer Engineering, National Chiao Tung University, Hsinchu 30010, Taiwan
[2]Philips Electronics Ltd., Shatin, Hong Kong
[3]Department of Photonics, Feng Chia University, Taichung 40724, Taiwan
[4]Industrial Technology Research Institute, Taiwan

DOI:10.1109/JPHOT.2020.2993031

Manuscript received April 11, 2020; revised April 30, 2020; accepted May 3, 2020. Date of publication May 7, 2020; date of current version May 29, 2020. This work was supported by the Ministry of Science and Technology, Taiwan, ROC, MOST-107-2221-E-009-118-MY3, MOST-108-2218-E-009-031, and ITRI subcontract project. Corresponding author: Chi-Wai Chow (e-mail: cwchow@faculty.nctu.edu.tw).

Abstract: We put forward and demonstrate a angle-of-arrival (AOA) based visible-light-positioning (VLP) system using quadrant-solar-cell (QSC) and third-order ridge regression machine learning (RRML) to improve the positioning accuracy.

Index Terms: Light emitting diode (LED), visible light communication (VLC), visible light positioning (VLP).

1. Introduction

Visible light communication (VLC) is an emerging technology for the next generation wireless communications [1–3]. Although the Global Positioning System (GPS) is very common nowadays; it is not suitable for indoor environments since the radio-frequency (RF) signals from satellites and mobile base stations are blocked. Visible light positioning (VLP) based on transmitting different identifiers (IDs) from different LED transmitters (Txs) was proposed [4]; however, its positioning resolution was limited in the range of meters. The proximity based VLP was proposed [5]; however, rolling-shutter camera based receiver (Rx) was needed for the detection. Fingerprinting based VLP was proposed in which specific signal detected was compared to the existing record for positioning [6]. However, it required stable received signals over time and a large data record. Time-of-arrival (TOA) as well as time-difference-of-arrival (TDOA) based VLP [7] can provide high positioning accuracy; however, they needed the Tx and Rx to be synchronized accurately. Trilateration based VLP using received-signal-strength (RSS) was proposed [8]; however, it needed multiple Txs. Recently, angle-of-arrival (AOA) schemes were proposed based on image sensor [9] or aperture-based Rx [10]. Another AOA VLP system using a quadrant photodiode angular diversity aperture receiver (QADA) is reported [11].

Here, we put forward and experimentally demonstrate an AOA VLP scheme based on a quadrant solar cell (QSC) and using 3rd order ridge regression machine learning (RRML) algorithm to

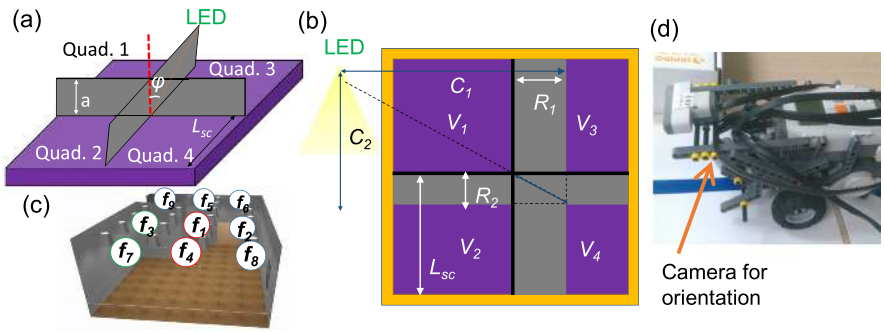

Fig. 1. (a) Principle of QSC for angular diversity AOA VLP Rx. (b) Top view of the QSC with different shadows produced by the barriers. (c) Unit cells with different beacon frequencies for whole area positioning. (d) One example of installing QSC on a robotic trolley.

improve the positioning accuracy. Experimental results show that root-mean-square (RMS) of average position error is reduced by 57.2% by using the RRML.

2. Algorithms and Experiment

We first transform a QSC into an angular diversity Rx for the AOA VLP. Here, the QSC is an integrated device with 4 identical crystalline silicon (Si) solar cells. It is also possible to use 4 Si-solar cell to construct the QSC. Two vertical small barriers of known height *a* are mounted on the QSC as shown in Fig. 1(a). These small barriers can change the amount of received light when the light source is located at different angles with respect to the QSC. In the AOA based VLP, the LED will cast different shadows onto the QSC when it is at different positions with respect to the QSC. By analyzing the received photo-currents at the 4 quadrants of the QSC, the position information can be obtained. If the QSC is rotated in the horizontal plane, the photo-currents at the 4 quadrants will change but the location is the same. Hence, it is important to define the orientation of the QSC at the beginning. A gyroscope can be applied to improve the VLP performance since the Rx orientation and the titling angles can be obtained. Besides, the height of the barrier will affect the performance of VLP since it will cast different shadows. If the barriers are too high, the shadow areas are too large; and these will not produce measureable photo-currents for the VLP. If the barriers are too low, the photo-currents generated from the 4 quadrants of the QSC will be similar; and this will affect the VLP accuracy.

The operation mechanism of the AOA VLP system is shown in Figs. 1(a) and (b). Fig. 1(c) illustrates using different unit cells with different LED emitted beacon frequencies for whole area positioning. Fig. 1(d) illustrates one application of installing the QSC in a robotic trolley. By using the front camera of the robotic trolley, the orientation of the QSC can be identified. The proposed VLP scheme could be installed in robotic trolley as illustrated in Fig. 1(d). The VLP trolley could be applied in hospitals or restaurants for medicine or food delivery. As shown in Figs. 1(a) and (b), when the LED is located at different incident angles with respected to the QSC, the light will cast different shadows of the barriers on the four quadrants. Hence the generated photo-current in the four quadrants will be different. Assuming the vertical distance between the LED and QSC is *A*, the horizontal distance between the LED and the edge of the shadow is C_i, where the subscribe *i* represents different quadrants of the QSC, and the height of the barrier is *a*. As illustrated in Fig. 1(b), the relative co-ordinates *X* and *Y* that specifies the location of the LED in relation to the center of the QSC can be expressed in Eq. (1), where V_i, L_{SC} and R_i are the photo-generated voltages, quadrant lengths, and shadow lengths, respectively. It is worth to mention that Eq. (1) describes the situation where the LED is at the top left corner of the QSC. It is not a general equation.

$$X = C_1 - R_1 = R_1\left(\frac{A}{a}\right) - L_{SC}\left(1 - \frac{V_3}{V_1}\right); \quad Y = C_2 - R_2 = R_2\left(\frac{A}{a}\right) - L_{SC}\left(1 - \frac{V_2}{V_1}\right) \tag{1}$$

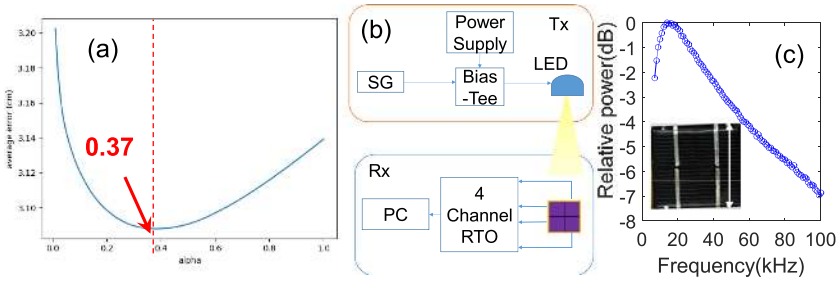

Fig. 2. (a) Average error of the test data against α. (b) Experimental setup of the QSC based AOA VLP system. (c) Measured frequency response of QSC. Inset: photograph of the QSC.

The incident angle φ between the LED and the center of QSC can be expressed in Eq. (2).

$$\varphi = \tan^{-1}\left(\frac{C_1 - R_1}{C_2 - R_2}\right) \tag{2}$$

In order to increase the position accuracy, third-order regression ML model [12] is employed. The model only needs to be trained once before deploying the positioning system. Let $\mathbf{W}_{\mathrm{ML}}$ be the weight vector to be solved, $\mathbf{\Phi}$ be the amplitude matrix, and D be the dimension, which equals four as there are 4 quadrants in the QSC. Eq. (3) shows the third-order regression ML model.

$$\mathbf{f} = w^{(0)} + \sum_{i=1}^{D} w^{(i)} q_i + \sum_{i=1}^{D}\sum_{j=1}^{D} w^{(ij)} q_i q_j + \sum_{i=1}^{D}\sum_{j=1}^{D}\sum_{k=1}^{D} w^{(ijk)} q_i q_j q_k = \mathbf{\Phi}\mathbf{W}_{\mathrm{ML}} \tag{3}$$

The amplitude $\mathbf{\Phi}$ is a two-dimensional matrix, and it can be expressed in Eq. (4), where N is the number of training data. In the experiment, we select 25 training locations inside the unit cell, and at each training location 20 sets of information (i.e., the four quadrants photo-generated voltages and x, y locations) are collected. The target vector $\mathbf{t}$ consists of the x- and y-coordinates.

$$\mathbf{\Phi} = [\phi_q(1), \phi_q(2), \ldots, \phi_q(N)]^{\mathrm{T}}; \phi_q(i) = [1, q_1(i), q_2(i), \ldots, q_3(i)q_4(i)q_4(i), q_4^3(i)] \tag{4}$$

Then, we apply the least squares with L2 regularization term scheme, also known as ridge regression, to obtain the weight vector $\mathbf{W}_{\mathrm{ML}}$. The error function is expressed as Eq. (5), where α is the hyper-parameter, which controls the relative importance of the regularization term when compared with the sum-of-squares error term.

$$E(w) = \sum_{n=1}^{N} [t_n - \mathbf{w}^{\mathrm{T}}\phi_q(n)]^2 + \alpha \mathbf{w}^{\mathrm{T}}\mathbf{w} \tag{5}$$

Here, we first apply the classical linear regression. By substituting the design matrix $\mathbf{\Phi}$ and target $\mathbf{t}$, $\mathbf{W}_{\mathrm{ML}}$ can be calculated as shown in Eq. (6).

$$\mathbf{W}_{\mathrm{ML}} = (\mathbf{\Phi}^{\mathrm{T}}\mathbf{\Phi})^{-1}\mathbf{\Phi}^{\mathrm{T}}\mathbf{t} \tag{6}$$

Besides the classical 3rd order regression, we also apply the 3rd order RRML algorithm, in order to obtain $\mathbf{W}_{\mathrm{ML}}$, the gradient of the error function should be equal to zero. Afterwards, we can obtain $\mathbf{W}_{\mathrm{ML}}$ as expressed in Eq. (7), where $\mathbf{I}$ is the unit matrix. By substituting the design matrix $\mathbf{\Phi}$ and target $\mathbf{t}$, $\mathbf{W}_{\mathrm{ML}}$ can be calculated. In order to get the optimal α in Eq. (5), we apply grid search [12] to optimize the hyper-parameter. The selection range of α is between 0 and 1, with an interval of 0.01; and the average error of testing data against α is shown in Fig. 2(a), showing the optimal $\alpha = 0.37$.

$$\mathbf{W}_{\mathrm{ML}} = (\alpha\mathbf{I} + \mathbf{\Phi}^{\mathrm{T}}\mathbf{\Phi})^{-1}\mathbf{\Phi}^{\mathrm{T}}\mathbf{t} \tag{7}$$

Since machine learning can learn the light intensity change at the 4 quadrants of the QSC at different environments, it can provide more accurate results than the traditional scheme by

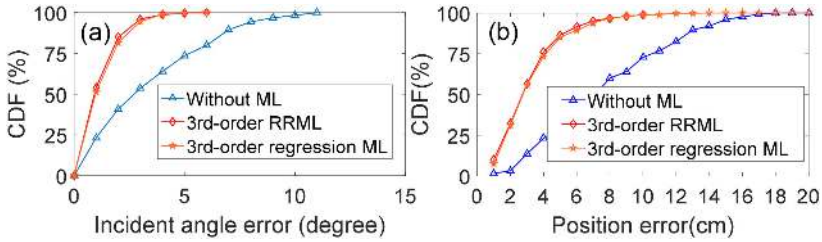

Fig. 3. Experimental CDF of (a) incident angle error and (b) position error of the QSC AOA VLP system.

only considering the shadow ratios. Using third-order ridge regression could further improve the accuracy. The experimental setup of the QSC based AOA VLP system is shown in Fig. 2(b). At the Tx side, an electrical beacon signal (sinusoidal frequency) generated by a signal generator (SC; Tektronix AFG3252C) is used to modulate a phosphor based white-LED. Direct-current (DC) from power supply is used to drive the LED via a bias-tee. At the Rx side, the four outputs from the QSC four quadrants are connected to a real-time oscilloscope (RTO, Tektronix MDO3024) to record the received photo-generated signals. Based on the received photo-generated signals of the QSC, the location information can be retrieved by using the above discussed algorithms implemented in Matlab and Python programs. It is worth to mention that the orientation of the QSC is important to obtain the correct position information.

Then, we study the optical-to-electrical (OE) conversion response of the QSC as shown in Fig. 2(c). The four quadrants show similar frequency responses with measured 3-dB OE bandwidth of ~50 kHz. The 3-dB bandwidths of the white-light LED and the QSC are about 1 MHz and 50 kHz respectively. Hence the limiting factor is from the QSC. The QSC bandwidth will affect the numbers of beacon frequency used for the whole positioning area. The low-frequency cut-off issue observed in the frequency response curve is typical regarding a solar cell. Inset of Fig. 2(c) shows the top view photography of the QSC. Its size is 4 cm x 4 cm. In this demonstration, a single 0.3 W LED is used to provide the illuminance in a unit cell with the cell dimension of 40 cm x 40 cm. The measured luminance at the center of the unit cell is about 450 lux, which is the typical luminance in a living room.

3. Results and Discussions

Then, we compare the experimental results of the QSC based AOA VLP system without ML, with the proposed 3rd order regression ML, and with the proposed 3rd order RRML. Figs. 3(a) and (b) show the incident angle φ error and the position error between the LED and the QSC respectively. As shown in Figs. 3(a) and (b), the improvement by applying the ML algorithms is significant. The maximum incident angle error (cumulative distribution function, CDF = 100%) of the incident angle is reduced from 10.4356° to 5.5593° by using the 3rd order RRML; showing an improvement of 46.7%. The RMS of average position errors are reduced from 7.2177 cm to 3.2025 cm, and to 3.0881 cm when using the 3rd order regression ML, and the proposed 3rd order RRML respectively; showing the improvements of 55.6% and 57.2% respectively.

Figs. 4(a)–(c) show the experimental performances of the QSC based AOA VLP without ML, with the proposed 3rd order regression ML, and with the proposed 3rd order RRML respectively; where the blue dots are the actual QSC locations and the red circles are the position errors. As illustrated in Fig. 4(a), in which the VLP is based on Eq. (1), the RMS position error is 7.2177 cm. As the positioning errors are too high, testing position separation of 10 cm is used. After applying the 3rd order regression ML and the 3rd order RRML as shown in Figs. 4(b) and (c), the RMS position errors are reduced to 3.2025 cm and 3.0881 cm respectively.

In this demonstration, the average illuminance inside the unit cell is about 335 lux, which is less than the required illuminance of 500 lux for a typical room. When the altitude of the LED increases, the received signal to noise ratio (SNR) by the QSC will decrease, and the positioning

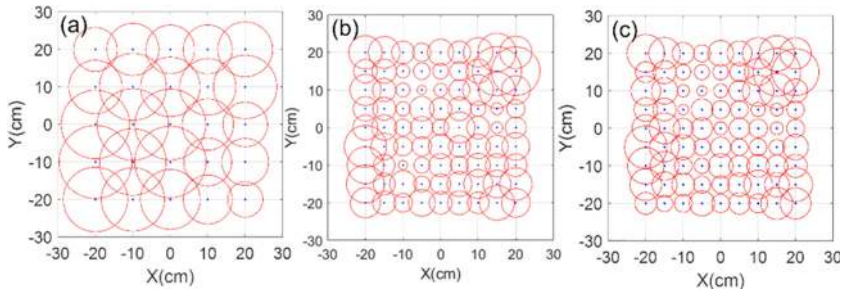

Fig. 4. Experimental AOA VLP performances (a) without ML, (b) 3rd order regression, (c) with the 3rd order RRML.

accuracy will also decrease. Positioning error may occur when the Rx is at the boundary between two VLP transmission lamps (i.e., boundary between unit cells). To reduce the positioning error at the boundary, the emitted optical signals from the two LEDs should be strong enough, or the distance between the LEDs should be close enough, so that the Rx can receive the two signals simultaneously. Here, the span in the LED arrangement could be 40 cm. We experimentally evaluated that if the tilting angle of the QSC is within $\pm 10^{o}$, the proposed VLP system can still work. More advanced mathematical model, such as deep neural network, could be used for the extreme conditions to improve the positioning accuracy. Fig. 1(c) illustrates using different unit cells with different LED beacon frequencies for whole area positioning. We experimentally evaluated that as long as the beacon frequency difference among the neighbor LEDs is large enough (the minimum frequency difference is 2 kHz), the VLP system can still work.

4. Conclusion

We proposed and demonstrated an AOA VLP scheme based on a QSC and 3rd order RRML algorithm. The RMS average position errors were reduced from 7.2177 cm to 3.2025 cm, and to 3.0881 cm when using the 3rd order regression ML, and the proposed 3rd order RRML respectively; showing the improvements of 55.6% and 57.2% respectively.

References

[1] C. W. Chow *et al.*, " Enabling techniques for optical wireless communication systems," *Proc. OFC* 2020, Paper M2F.1.
[2] H. H. Lu, Y. P. Lin, P. Y. Wu, C. Y. Chen, M. C. Chen, and T. W. Jhang, "A multiple-input-multiple-output visible light communication system based on VCSELs and spatial light modulators," *Opt. Express*, 22, pp. 3468–3474, 2014.
[3] C. T. Tsai, C. H. Cheng, H. C. Kuo, and G. R. Lin, "Toward high-speed visible laser lighting based optical wireless communications, "*Progress in Quant. Electron.*, vol. 67, pp. 100225, 2019.
[4] S. Ayub, S. Kariyawasam, M. Honary, and B. Honary, "Visible light ID system for indoor localization, "in *Proc. ICWMMN* 2013, pp. 254–257.
[5] C. Y. Xie, W. P. Guan, Y. X. Wu, L. T. Fang and Y. Cai, "The LED-ID detection and recognition method based on visible light positioning using proximity method," *IEEE Photon. J.* 10, 7902116 (2018).
[6] C. Zhao, H. Zhang and J. Song, "Fingerprint and visible light communication based indoor positioning method, "in *Proc. ICAIT*, 2017, pp. 204–209.
[7] P. F. Du, S. Zhang, C. Chen, A. Alphones, and W. D. Zhong, "Demonstration of a low-complexity indoor visible light positioning system using an enhanced TDOA scheme," IEEE Photon. J., vol. 10, pp. 7905110, 2018.
[8] C. W. Hsu *et al.*, "Visible light positioning and lighting based on identity positioning and RF carrier allocation technique using a solar cell receiver, "*IEEE Photon. J.*, vol. 8, 7905507, 2016.
[9] M. H. Bergen, X. Jin, D. Guerrero, H. A. L. F. Chaves, N. V. Fredeen, and J. F. Holzman, "Design and implementation of an optical receiver for angle-of-arrival-based positioning, "*J. Lightw. Technol.*, vol. 35, pp. 3877–3885, 2017.
[10] H. Steendam, "A 3-D positioning algorithm for AOA-based VLP with an aperture-based receiver, "*IEEE J. Select. Areas in Comm.*, vol. 36, pp. 23–33, 2018.
[11] S. Cincotta, C. He, A. Neild, and J. Armstrong, "High angular resolution visible light positioning using a quadrant photodiode angular diversity aperture receiver (QADA), "*Opt. Express*, vol. 26, pp. 9230–9242, 2018.
[12] S. Raschka and V. Mirjalili, Python Machine Learning: Machine Learning and Deep Learning with Python, scikit-learn, and TensorFlow (Packt Publishing, 2017).